NASA Technical Paper 1381

Lidar Backscattering Measurements of Background Stratospheric Aerosols

Ellis E. Remsberg, G. Burton Northam,
and Carolyn F. Butler

FEBRUARY 1979

NASA

NASA Technical Paper 1381

Lidar Backscattering Measurements of Background Stratospheric Aerosols

Ellis E. Remsberg and G. Burton Northam
Langley Research Center
Hampton, Virginia

Carolyn F. Butler
Old Dominion University Research Foundation
Norfolk, Virginia

National Aeronautics
and Space Administration

**Scientific and Technical
Information Office**

1979

SUMMARY

Background stratospheric aerosols typically yield scattering ratios R of the order of 1.10 at 20 km for a ruby lidar system. Background aerosol amounts inferred from lidar backscatter measurements are affected by both random and systematic uncertainties. In this report, the calibration and data-analysis procedures for the NASA Langley 48-inch lidar system are discussed. These procedures have been supported by obtaining concurrent dustsonde and lidar profiles of stratospheric aerosols during a comparative experiment conducted in San Angelo, Texas, in May 1974. A comparison of profiles obtained by these two techniques is within the accuracy of the two measurements below 23 km. At higher altitudes the comparison is improved when an altitude-dependent aerosol size distribution is considered. Lidar data from the Texas experiment yielded an average random uncertainty in R of 2.5 percent, with uncertainties in molecular density being most important. The systematic uncertainty in R due to the lidar profile normalization procedure is estimated from aerosol model calculations to have been 5 percent. For the Texas experiment the aerosol component of the atmospheric backscatter at 20 km contains random and systematic uncertainties of 35 and 63 percent, respectively.

INTRODUCTION

Various remote measurement techniques are being used to characterize the stratospheric-aerosol layer. One such technique is the use of lidar systems. A lidar measure of the aerosol concentration is the scattering ratio R, that is, the total atmospheric backscatter divided by the molecular backscatter. The quantity $R - 1$ is the fraction of the atmospheric backscattering that is due to aerosols. Efforts to monitor the seasonal and annual variability of stratospheric aerosols have been undertaken at a number of lidar installations. Fox et al. (ref. 1), Remsberg and Northam (ref. 2), and Russell et al. (ref. 3) have presented data on $R - 1$ from 1964 to 1974 to show the decreasing trend in aerosol loading at the 20 km altitude since the eruption of Mt. Agung in 1963. (See fig. 1.) In figure 1 the vertical bars represent the range of scattering-ratio data over the time periods within the horizontal bars. A background level of 1.20 to 1.05 in R prevailed from 1971 to 1974. Up to 1974 the aerosol loading had either leveled off or was still declining. The occurrence of the Fuego volcanic event in October 1974 has made it difficult to know whether or not a steady-state stratospheric-aerosol level had been reached during the summer of 1974. Thus, the term "background aerosol amount" is still a relative one. The decay of the Fuego aerosol layer has been discussed by McCormick et al. (ref. 4); during 1977 the layer approached the pre-Fuego levels once again. Studies of trends in the background aerosol amount require data sets taken periodically at a number of geographic locations.

The accuracy of the lidar measurements in figure 1 and the ability to intercompare them depend heavily on the individual system calibrations and data-analysis procedures. Northam et al. (ref. 5) have reported on a Wyoming

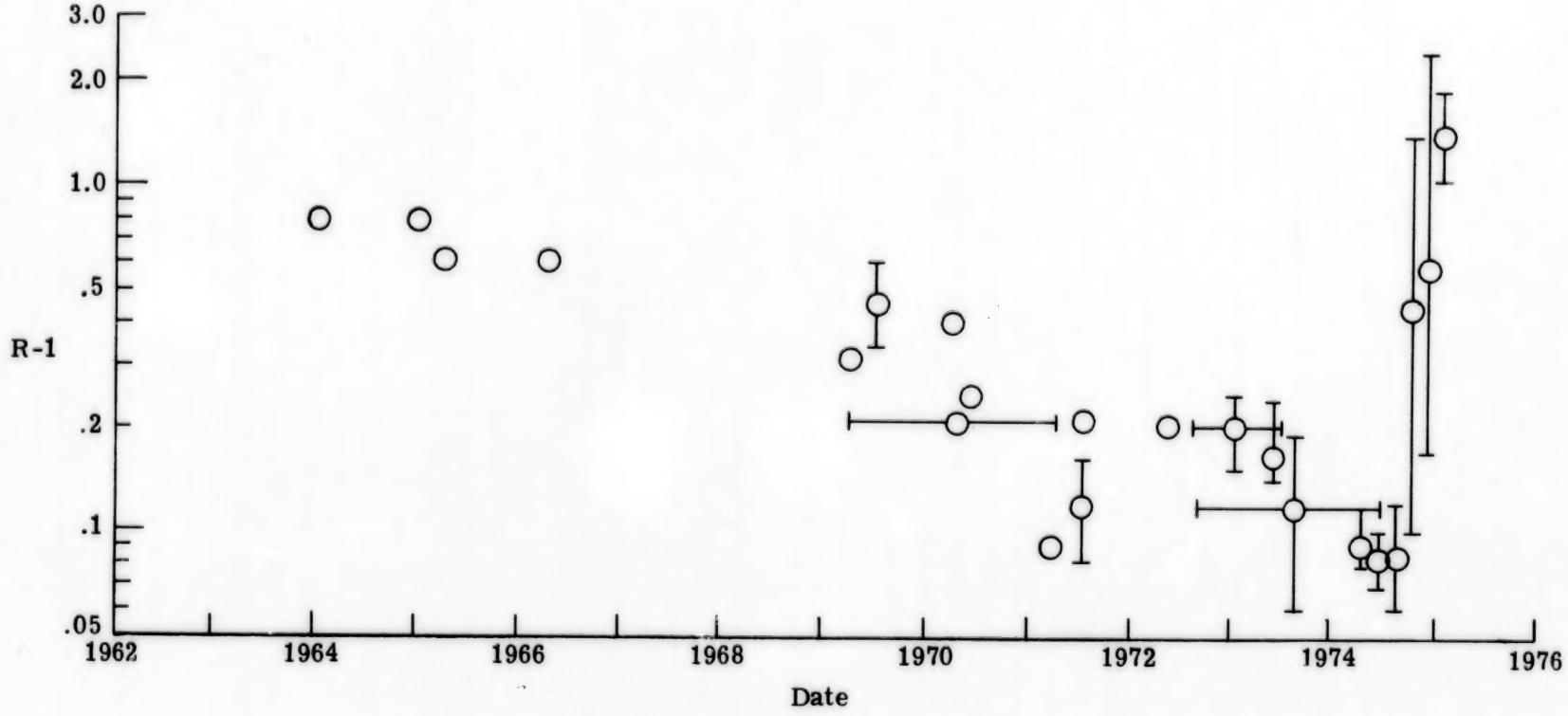

Figure 1.- Average maximum scattering ratio for 20 km altitude.
(Data represented by ○ taken from ref. 2.)

comparative experiment (WCE) at Laramie, Wyoming, in 1972 using the Langley 48-inch lidar system and the University of Wyoming dustsonde measurements. That particular experiment indicated agreement between the relative profile shapes obtained by the two methods, but further refinements in the lidar calibration and data-analysis procedures were necessary before systematic error estimates could be made. Further calibrations of the Langley 48-inch lidar system were performed, and a Texas comparative experiment (TCE) was conducted on May 7 and 8, 1974, at San Angelo, Texas. This report describes the refinements in the data-reduction procedures employed in that experiment, and the various error sources are described in some detail. The results of the TCE are then discussed, including stratospheric-aerosol profiles as measured by a balloon-borne in situ particle counter and by backscattered light from the ground-based lidar operating at a wavelength of 0.694 μm. Aerosol extinction estimates derived from the lidar profiles are also compared with extinction data inferred from searchlight measurements of the aerosol layer. The implications for the monitoring of long-term aerosol trends by lidar are reviewed.

The authors wish to express their gratitude to Professor J. Rosen of the University of Wyoming for conducting the dustsonde launch at San Angelo, Texas, and for supplying his reduced data. M. Patrick McCormick and William H. Fuller, Jr., of the Langley Research Center participated in the coordination of the TCE, and W. Hunt, C. Bartusiak, and F. Diehl of Wyle Laboratories, Hampton, Virginia, assisted with the lidar measurements at both San Angelo, Texas, and Hampton, Virginia. Dr. S. K. Poultney of Perkin Elmer Corporation, Norwalk, Connecticut (formerly of the Old Dominion University Research Foundation) and W. Hunt performed the photomultiplier-tube calibrations by simulating the lidar returns with light-emitting diode pulses.

SYMBOLS

E	laser output energy per pulse, J
f	backscattering function, m^{-1}-sr^{-1}
k	constant in equation (1)
N	number density, m^{-3}
n	refractive index
P(180)	backscattering phase function
q	transmissivity of model atmosphere
R	scattering ratio
r	particle radius, μm
T	turbidity
T(180)	backscatter turbidity

V	voltage of photomultiplier, V
z	altitude, m
α	aerosol size parameter
β	total scatter function, m^{-1}
γ	relative backscatter efficiency
η	geometric cross section, m^2
λ	wavelength, μm
ν	size distribution parameter
σ	backscattering cross section, $m^2\text{-}sr^{-1}$
Ω	solid angle, sr

Subscripts:

a	aerosol
d	dustsonde
m	molecular

Abbreviations:

TCE	Texas comparative experiment
WCE	Wyoming comparative experiment

DESCRIPTION AND CALIBRATION OF LIDAR SYSTEM

The Langley 48-inch lidar system (refs. 5 and 6) consists of a pulsed laser transmitter and a telescope receiver with parallel alignment of the optical axes. (See fig. 2.) The laser pulse of nearly monochromatic light is scattered by aerosols and molecules as it propagates through the atmosphere. A small percentage of this light is backscattered into the telescope which directs the light through optical filters onto one or more of the four photomultiplier tubes. The beamsplitter directs fractions of the total incident light energy to the first three tubes, while the fourth tube is a photon counting detector. The detector package is triggered at the time of the laser firing, and each photomultiplier tube measures the backscattered photons or energy at appropriate subsequent time intervals. In this manner a range resolved measure of the total backscatter, due to both aerosols and molecules, is obtained.

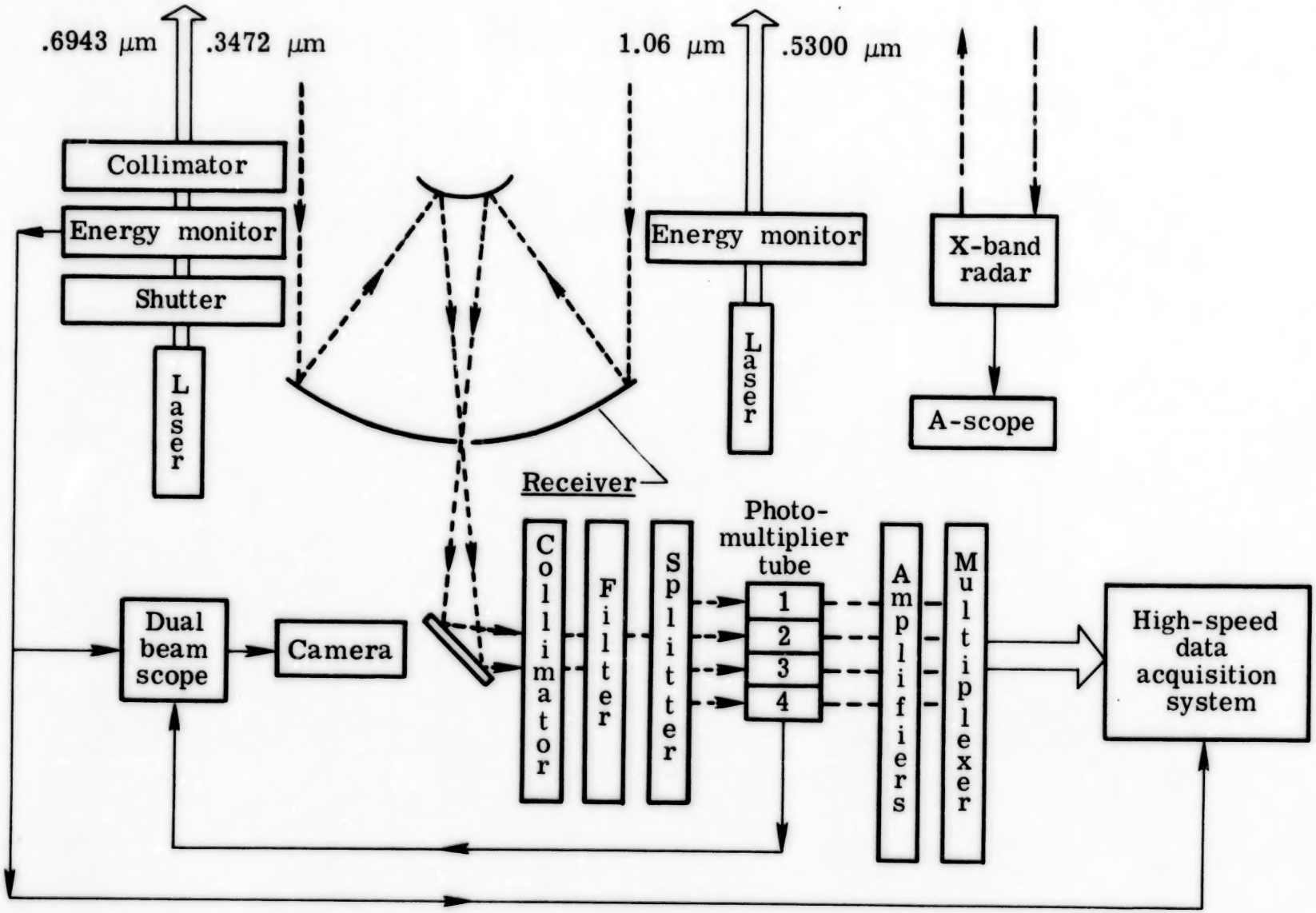

Figure 2.- Langley 48-inch lidar system.

The transmitter is a temperature-stabilized ruby laser, operating at 2.5 to 3.0 J at 4 pulses per minute. The transmitter is equipped with a doubling crystal, allowing for two wavelength outputs (0.347 and 0.694 μm). A neodymium-glass laser (1.06 and 0.53 μm) is available as an auxiliary transmitter. This report discusses only returns obtained at 0.694 μm. The receiver is an f/10 Cassegrain 1.32-m (48-in.) diameter telescope. The total system also includes a pulse counter, analog-to-digital converter, tape recorder, and computer subsystems. A calibrated photodiode samples a portion of the laser output energy and also provides a zero time pulse that initiates the system timing circuits. The photomultiplier outputs are amplified, analog-to-digitally converted at a rate of 10 MHz with 8-bit 2048-word capability, and placed in buffer memory. The computer accesses the buffer memory at a 1 MHz rate and stores the data on magnetic tape.

In the WCE, complete profiles were obtained by combining three data segments which were taken at successive times. That technique imparted a potential error to the profile due to the temporal changes occurring in the atmospheric-aerosol returns from each altitude segment. To overcome this problem, a sequentially switched three-tube high-dynamic-range analog detector package was used each laser firing in the TCE to survey the 10 to 30 km altitube profile. Potential nonlinearities in the detector tubes and amplifiers were detected by simulating the backscattered laser pulse with a light-emitting diode and by comparing the three channels. Linear tube response is a necessity for combining the signals measured with the three tubes and also for the subsequent normalization of the total profile to the expected molecular return at a given altitude. As pointed out by Pettifer (ref. 7), signal-induced noise results in a residual nonlinearity that may have a significant effect on the final lidar profile. This effect is fully discussed for the Langley 48-inch lidar system by Hunt and Poultney in reference 8. Photomultiplier-tube response was checked for nonlinearities both before and after the TCE. A calibration of the 48-inch lidar data-acquisition system was also performed. Due to a faulty electrical alignment, the analog-to-digital converter (ADC) response was nonlinear, but it was accounted for by calibration of the ADC system.

Up to 10 background measurements were performed before and after each set of 50 to 100 laser firings in the TCE. Part of the background signal resulted from the ruby fluorescence return due to aerosols at low altitudes. This background component occurs because the laser and telescope for the 48-inch system are separated by 1 m; this proximity resulted in overlapping of the transmitted and received images at $Z = 1/2$ km for a 4 mrad field of view. This low overlap altitude was just where aerosols tend to have their highest concentration in the mixed layer and, thus, where background fluorescence was a problem. That part of the return was simulated by firing the laser at reduced Pockel cell voltages for which no lasing pulses were emitted. Those background returns varied slightly from one set of laser firings to another; and, since they were superposed on the stratospheric returns at altitudes where profile normalization was often attempted ($Z = 28$ to 31 km), adjacent sets of background returns were averaged and subtracted from each corresponding set of atmospheric returns. (Since the TCE, a rotating shutter has been installed to eliminate the fluorescence return.) Another source of background signal was the slowly varying "dc drift" due to the dc coupled amplifier and to low light levels being passed by the spectral filters. An uncertainty of $\pm 1/2$ count was also present for the

system itself because of an inability to record fractional counts. At the upper end of each of the three photomultiplier-tube profiles, the ratio of actual received signal to that measured as dc background became small. Any drift in the dc level was therefore important and was considered by occasionally comparing photomultiplier-tube output curves for any changes in gain.

DATA ERROR ANALYSIS

A typical lidar-return curve from the atmosphere for the TCE is given in figure 3. This curve represents range-corrected relative signal Z^2V/E as a function of range Z, where V is the voltage of the return signal and E is the laser output energy. The molecular-return curve in figure 3 represents the calculated return signal which would be expected from just the molecules in the atmosphere at the time of the TCE. The difference between the two curves, then, is a measure of the aerosols or clouds that were present. Since the

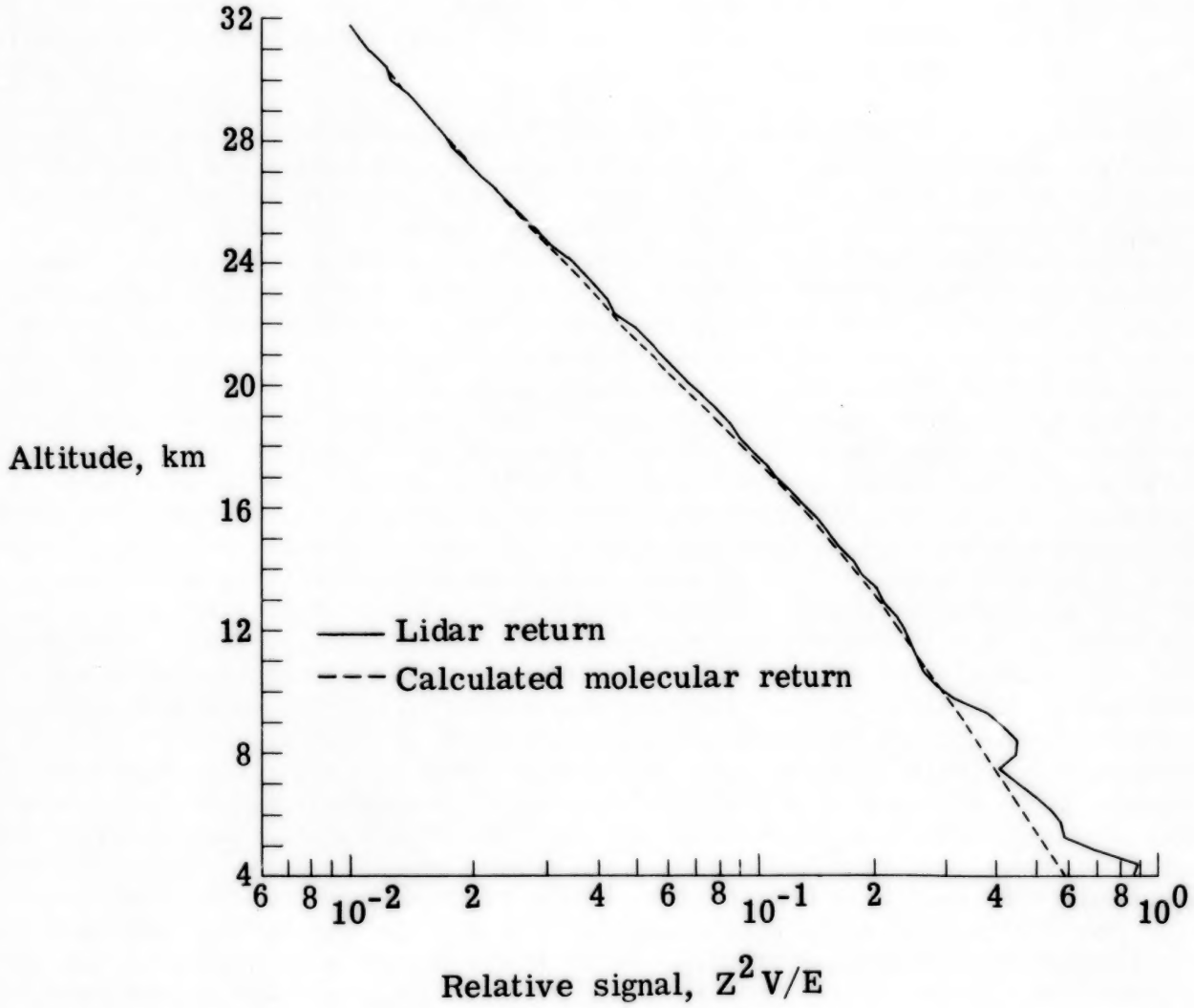

Figure 3.- Range-corrected lidar returns from TCE. 0330 to 0400 MDT; 100 shots.

atmospheric-signal profile $V(Z)$ varies by over three orders of magnitude from 4 to 30 km, three photomultiplier tubes were required to provide the dynamic range necessary to measure the backscattered signal accurately. Techniques for generating complete profiles (fig. 3) from those measurements are discussed in the following section.

Background and Combination Effects

At the time of the WCE (ref. 5), the data-acquisition program limited the data return to 700 words, corresponding to a range increment of 10.5 km. For returns up to 30 km, it was necessary to record sets of three 10.5 km altitude segments of data at successive times by changing the initial delay on the photomultiplier-tube detector package. In order to obtain a single continuous profile, the altitude regions of overlap between sets of adjacent segments were used to combine those averaged segments with each other, and the result was fit to a polynomial. In the overlap regions, any pronounced features either due to fluorescence and detector background or to aerosol layer structure could have produced significant errors in the final combined profile. Real structural changes in the atmospheric returns, though infrequent, have been observed during a period of several hours.

The sequence of data handling for the TCE proceeded as follows. A multiplexer was used to switch-in the three photomultiplier tubes, and 2048 words were recorded to yield a total 30 km profile for each laser firing. Each segment was corrected for variations in background effects and laser power. To determine background effects, 10 measurements were taken and averaged. Since signals from each of the three photomultiplier tubes decrease with range, the ratios of signal to background approach unity and, therefore, the data become increasingly more sensitive to background subtraction (fig. 4). As a result, a linear approximation was made to the second half of these returns to eliminate the effects of system noise fluctuations in the low-level background signal. Then, this approximation to the background was subtracted from the averaged set of stratospheric returns, and the resultant profile segments were range corrected. Due to the different amplifier gains and light levels for the three photomultiplier tubes, the data segments still had to be combined into one complete profile. To minimize uncertainties in atmospheric returns at the gain-switched altitudes, two sets of returns (primed and unprimed segments in fig. 5) were taken at about 15-min time intervals with combination points at different altitudes. Continuous portions of one profile overlapped the gain-switched altitudes of the other profile, and any signal perturbations were more easily discerned by comparing both profiles. The problem of rapidly (within 15 min) changing signal perturbations between adjacent sets of data still remained, however, as in the case of a thin cirrus feature moving across the field of view. Visual inspection of the data at the time of the measurement identified those few cases, and profile data were obtained then with just a single photomultiplier tube over a more limited altitude range. Once the data from the three photomultiplier tubes were combined, the profile was further averaged, this time over altitude. Typically, 30 altitude points were averaged to give a height resolution of 0.45 km. No other smoothing was applied to the data to achieve the final profiles.

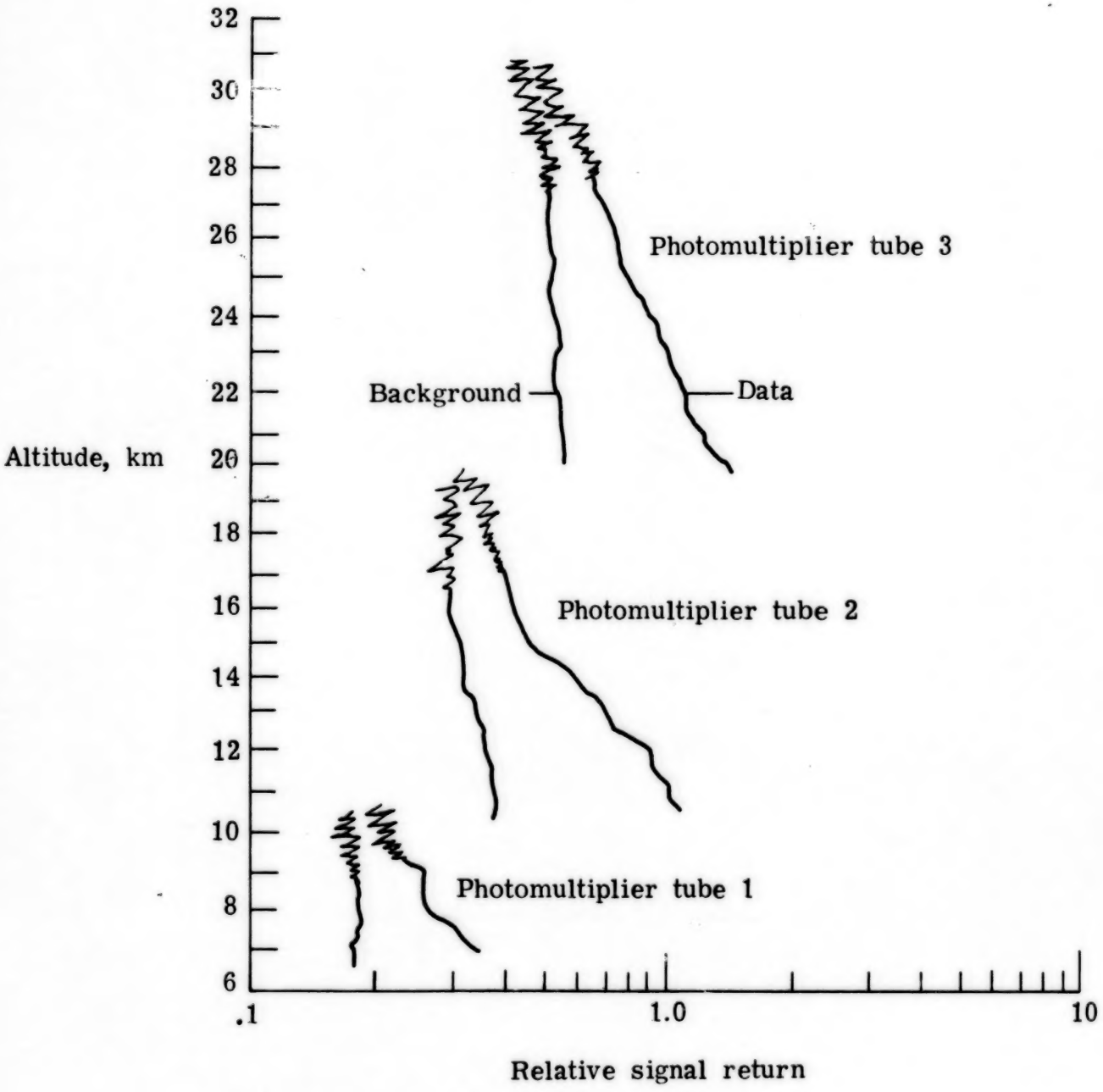

Figure 4.- Background and lidar returns for three altitude ranges.

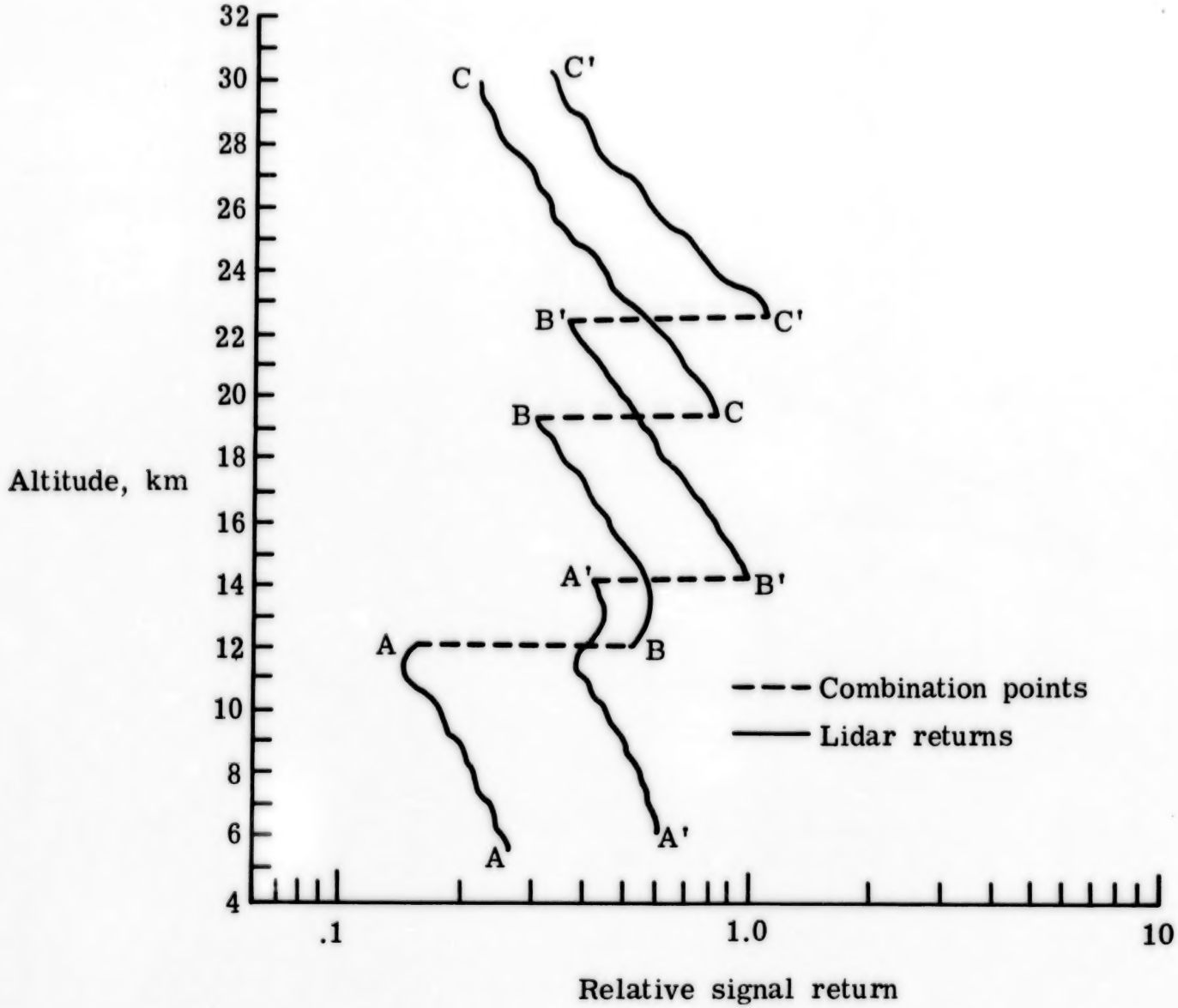

Figure 5.- Procedure for combining return signals.

Random and Systematic Errors

Northam et al. (ref. 5) have discussed the lidar equation and its subsequent use in the calculation of scattering ratio R and aerosol backscattering function f_a. The ratio R of the signal given by the lidar equation to the calculated molecular or clear-air return is given by

$$R = k \frac{Z^2 V(Z)}{f_m(Z) q^2(Z)} = 1 + \frac{f_a(Z)}{f_m(Z)} \tag{1}$$

where q^2 is a two-way atmospheric attenuation factor, Z is altitude, V is return signal, and f_m and f_a are the molecular and aerosol backscattering functions, respectively. The quantity $f_m(Z)q^2(Z)/Z^2$ is proportional to the expected molecular lidar return. Since $f_m = \sigma_m N_m(Z)$, where N_m is molecular number density and σ_m is the molecular backscattering cross section, the aerosol portion of the scattering ratio $f_a(Z)/f_m(Z)$ can be calculated. Since it is difficult to determine remotely whether any altitude region is free of aerosols, the constant k that relates the expected molecular return to the total lidar signal return was evaluated on the basis of assuming only molecular scattering for altitudes between 28 and 31 km where aerosols often are at a minimum (refs. 3 and 5). This assumption forces R to be unity at those altitudes.

Figure 6 shows the scattering-ratio profile derived from data in figure 3 for an average of 100 lidar returns. This averaging procedure gives better than 2-percent standard deviation in the scattering ratio for altitudes up to 30 km over 25 min. The molecular-return profile was calculated by using temperature and pressure data obtained at 0200 MDT at San Angelo, Texas. Error bars in figure 6 represent 95-percent confidence intervals for the random changes in the scattering-ratio data. These intervals do not increase uniformly with altitude because the signal-to-noise ratio for each photomultiplier tube was about the same. A bulge in the scattering-ratio profile occurs between 18 and 24 km, but its peak value is only 1.07 which is representative of relatively low aerosol content. Equation (1) can be rearranged and used to calculate the aerosol backscattering function

$$f_a(Z) = (R - 1)\sigma_m N_m(Z) \tag{2}$$

which is plotted in figure 7. Since f_a may be represented as the product of an effective aerosol backscatter cross section σ_a and particle concentration N_a (ref. 5), profiles developed herein may be used to infer the aerosol number density as a function of altitude provided σ_a is known. The conversion of the lidar returns to a scattering-ratio profile and then to an aerosol backscattering-function profile was subject to several possible errors: measured temperature profile, attenuation model, and normalization procedure. Each of these is discussed in turn.

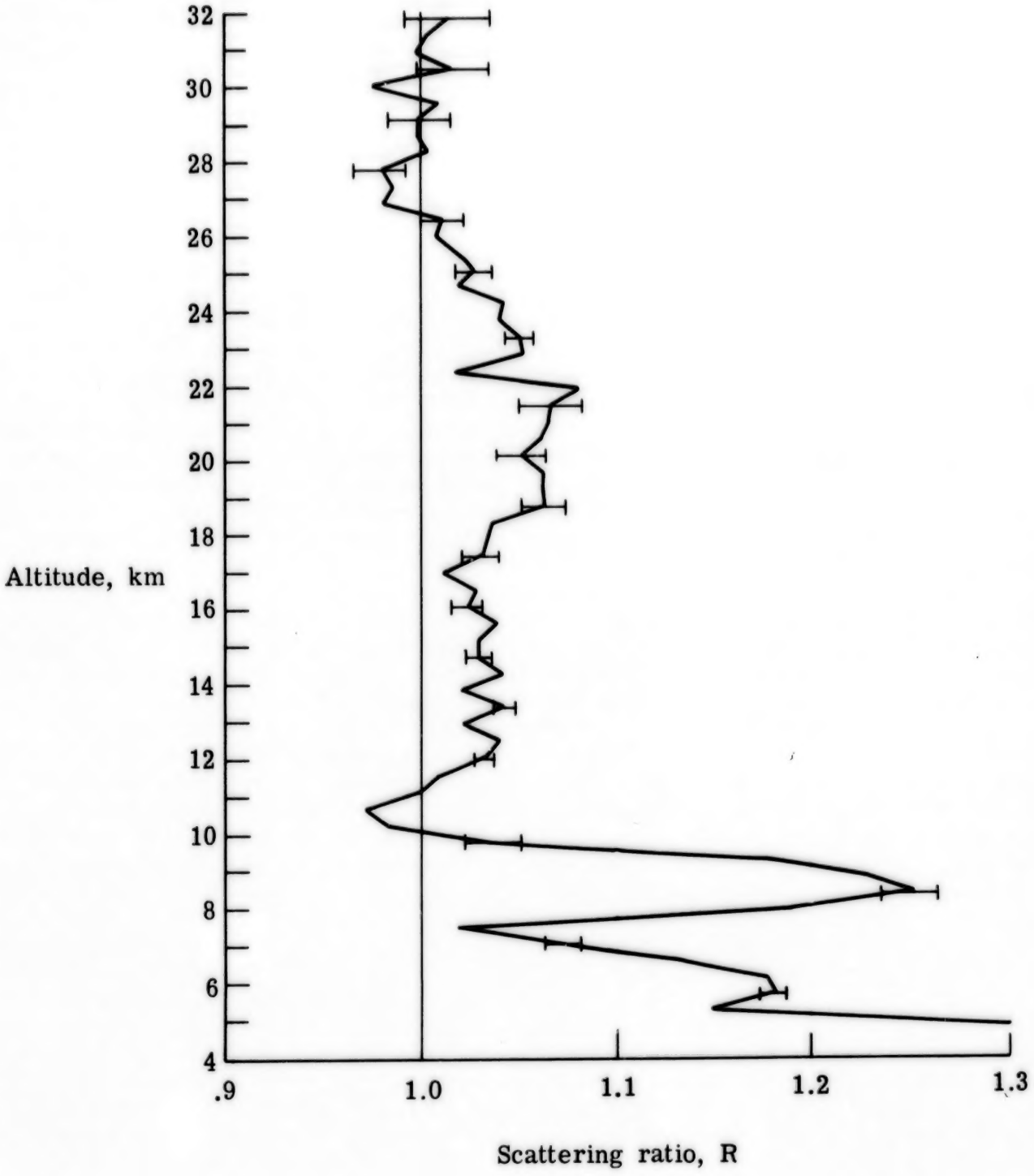

Figure 6.- Scattering-ratio profile from TCE. 0330 to 0400 MDT; 100 shots; 95-percent confidence intervals represented by horizontal bars.

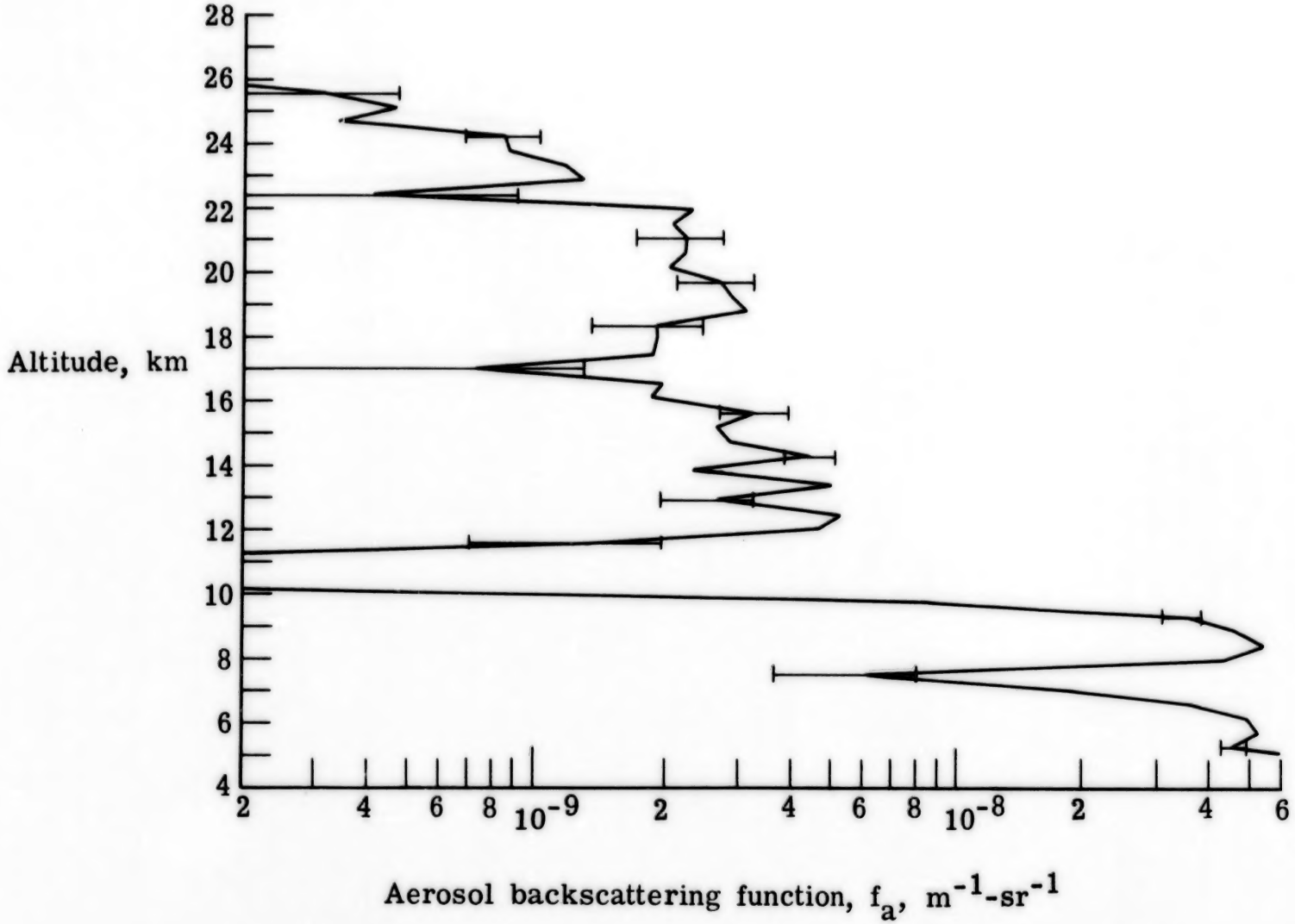

Figure 7.- Backscattering-function profile from TCE. 0330 to 0400 MDT; 100 shots; 95-percent confidence intervals represented by horizontal bars.

The effect of using different molecular-density profiles for calculating a scattering-ratio profile is shown in figure 8 for another lidar data set taken on May 5, 1974. Radiosonde data were obtained at both San Angelo, Texas, and Midland, Texas (about 150 km to the northwest) about 3 hr after the lidar measurements. Due to differences in temperature and pressure from the two locations, R was found to vary from 0 to 3 percent in this profile comparison, with the average being 1 percent. This uncertainty may, in fact, be due to the relative radiosonde density error of 1 percent (ref. 3). Thus, uncertainties in air density are comparable to the 2-percent random signal error. Since the maximum contribution to R from aerosols was about 7 percent in the stratosphere at that time, variations in molecular density were significant.

Intervening atmospheric species may absorb a portion of the laser beam as well as scatter the incident light in all directions. Attenuation profiles for a particular wavelength are proportional to the number density of neutral molecules, aerosols, and ozone; the latter is especially important for wavelengths shorter than 0.32 μm. Molecular scattering and ozone absorption remain nearly constant from year to year, but the aerosol or Mie scattering depends on the current particle size distribution and composition.

Values for the two-way attenuation $q^2(z)$ applied in figure 6 were approximated from Elterman's tabulation at 0.70 μm (ref. 9). No attempt was made to correct the Elterman attenuation data for the aerosol content being measured because simulations indicate that for aerosol amounts in the stratosphere (R = 1.10) just before May 1974 an error in R of only 1 percent occurred if the aerosol attenuation was neglected altogether (ref. 3). Elterman's aerosol attenuation coefficients (ref. 10) derived from data taken after the volcanic eruption of Mt. Agung in 1963 are not applicable to an analysis of background aerosol levels.

The random uncertainties are summarized as a signal error of 2 percent, a molecular density error of 1 percent (range of 0 to 3 percent), and an attenuation error of 1 percent. The root-mean-square value of these uncertainties equals 2.5 percent.

In determining the magnitude of the scattering ratio with equation (1), one must assume that f_a has a known minimum value (normally taken to be zero) at some altitude. Russell et al. (ref. 11) found that the region just above the tropopause at Laramie, Wyoming, is often aerosol free, but this characterization cannot be generalized for other locations because the occurrence of aerosol-free regions near the tropopause is effectively influenced by the tropospheric weather patterns and the position of the jet stream. Theoretical one-dimensional studies of processes affecting the background stratospheric-aerosol layer indicate that the major constituent, sulfuric acid aerosols, should be depleted because of "washout" near the tropopause and because of evaporation above about 30 km (ref. 12). In the present analysis the region between 28 and 31 km was selected as the normalization region. That choice is examined further in the following section.

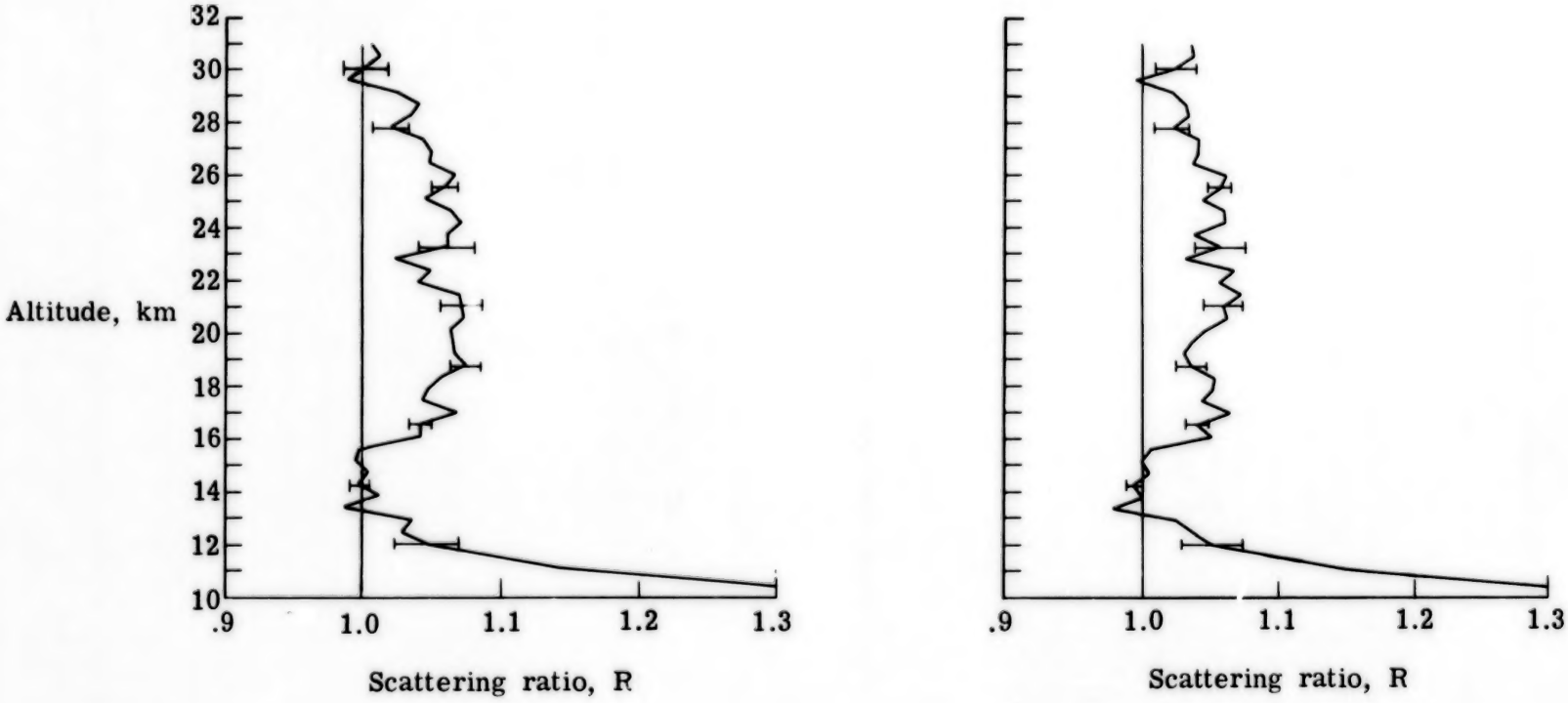

Figure 8.- Scattering ratio obtained with temperature profiles from Midland, Texas, and San Angelo, Texas, for May 5, 1974.

TEXAS COMPARATIVE EXPERIMENT

Lidar-Dustsonde Comparison

The time line for the lidar measurements and for the dustsonde launch for the TCE is shown in table I. Over 800 laser firings were made on a schedule to include the dustsonde launch and measurements. The dustsonde, launched at 0200 MDT, ascended through the lower stratosphere at approximately 0330 to 0400 MDT in coincidence with the averaged lidar data in figures 6 and 7. The dustsonde measured the particle number density N_d directly using two detector channels, one (channel A) to discriminate particles larger than 0.15 μm in radius and the other (channel B) for particles larger than 0.25 μm. For each channel, 500 particle counts were registered before a data point was recorded; the counting error in N_d according to Poisson statistics was 4 percent. Hofmann et al. (ref. 13) give an uncertainty in N_d for channel A of ±10 percent due to all instrumental errors. The altitude resolution at 20 km was 0.5 km for channel A and 0.7 km for channel B, values which are comparable to the 0.45 km value for the lidar profile. Details of the general operation and calibration of the particle counter have been described in references 5 and 13.

TABLE I.- LIDAR AND DUSTSONDE MEASUREMENTS

FOR TEXAS COMPARATIVE EXPERIMENT

Date	Time, MDT	Number of shots
Lidar soundings		
May 7, 1974	2035	50
	2102	50
	2223	60
	2333	300
May 8, 1974	0122	70
	0158	100
	0236	130
	0328	100
Dustsonde launch		
May 8, 1974	0200	

In figures 9 and 10 the aerosol backscattering-function profile is compared directly with particle counts N_d measured with the dustsonde. Error bars on f_a represent 95-percent confidence intervals determined from the lidar signal statistics which vary according to the signal-to-noise ratio in each of the photomultiplier tubes. If the 1-percent random error in the molecular density

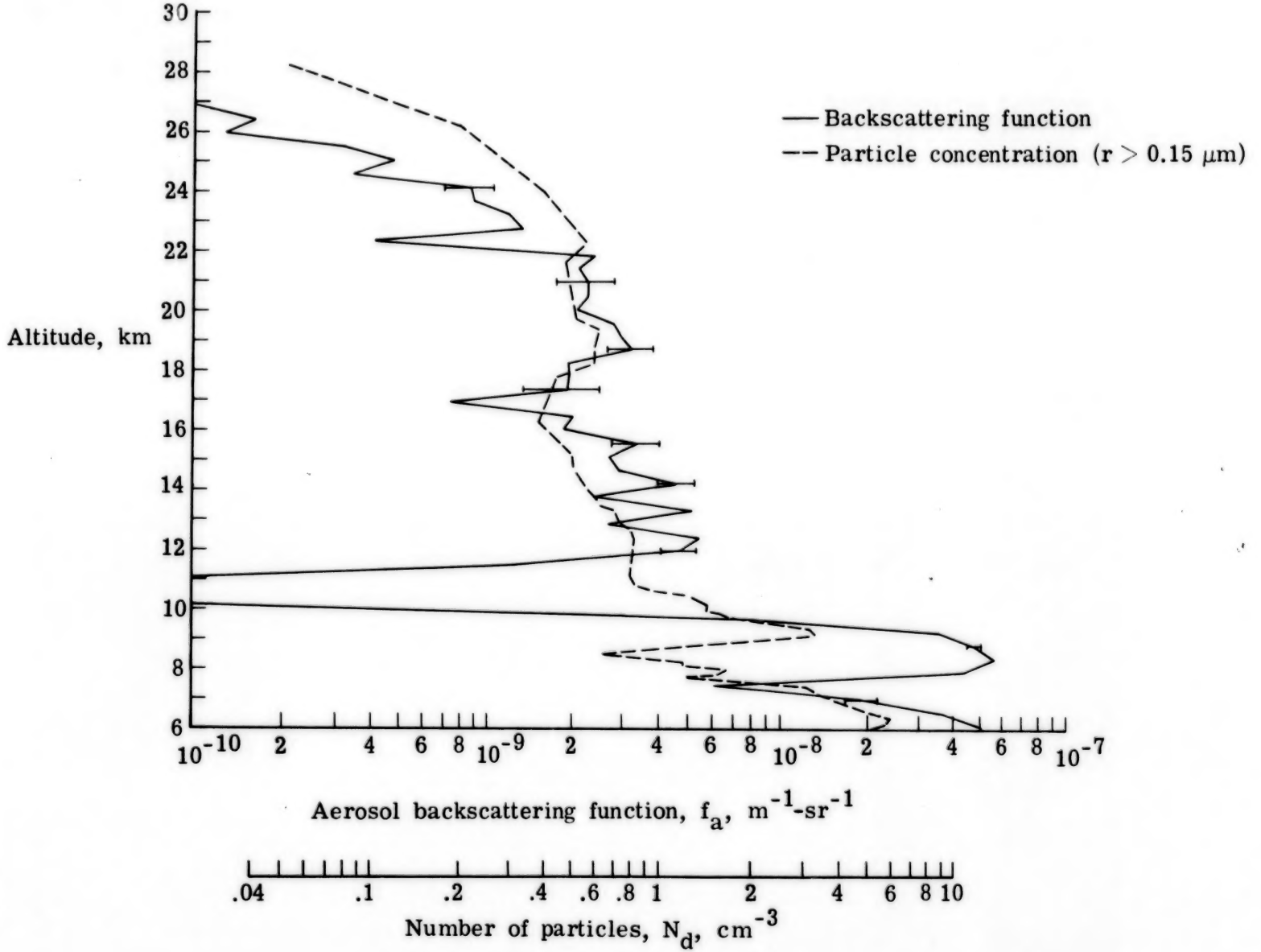

Figure 9.- Comparison of lidar and dustsonde profiles for particles with radii greater than 0.15 μm from TCE.

were included, the total standard random error in f_a would be 35 percent at 20 km. Since initially only a relative profile comparison was sought, the dustsonde and lidar profiles in figures 9 and 10 were normalized at one altitude, 20 km. Inherent in this method of profile comparison is the assumption that the σ_a is constant with altitude in the stratosphere. If it is further assumed that the dustsonde and lidar are responsive to the same portion of the particle size distribution, then $N_a = N_d$. The comparison in figure 9 for particles with radii greater than 0.15 μm shows that 1 particle per cm^3 corresponds to a value of $f_a = 4 \times 10^{-9}$ m^{-1}-sr^{-1}. Minima occur in both profiles between 15 and 17 km, and enhancements exist from 17 to 22 km. The stratospheric aerosol layer exhibited a maximum concentration of 0.6 particle per cm^3 at 19 km. If the standard error of 10 percent for N_d is considered, the relation between the measurement techniques is not within the error bars above 23 km. This discrepancy is addressed later in this section. Figure 10 shows the same comparison for particles with radii greater than 0.25 μm. Here the correlation is better, especially at the higher altitudes, indicating that the lidar wavelength, 0.694 μm, may exhibit sensitivity to the particle size distribution with height. Particles detected in channel B exhibit correspondence when 1 particle per cm^3 is equivalent to $f_a = 1.8 \times 10^{-8}$ m^{-1}-sr^{-1}. Values for σ_a derived from figures 9 and 10 are 4×10^{-15} m^2-sr^{-1} and 1.8×10^{-14} m^2-sr^{-1}, respectively. At altitudes closer to the tropopause, these values of σ_a do not apply since cirrus particle composition, size, and shape are considerably different from those for the aerosols.

Now, consider the two assumptions applied to the TCE data analysis: (1) that the 28 to 31 km region for normalization was aerosol free and (2) that the quantity σ_a was constant between 11 and 28 km.

Effect of Normalization Criterion

There is no evidence from figures 6 and 8 to suggest that a different altitude, between 10 and 31 km, would have been better than the 28 to 31 km range for normalization, although Russell et al. (ref. 3) present data that indicate an average underestimate in R of 3 percent if 30 km were chosen instead of 12 km. Still, it is possible that no altitude between 10 and 31 km is really free of aerosol.

Aerosol model calculations in reference 14 by Pinnick et al. (see their model N_1 with refractive index 1.40 - 0i) indicate that for $N_d = 0.06$ cm^{-3} at 28.0 km in figure 9, one could expect $f_a = 5 \times 10^{-10}$ m^{-1}-sr^{-1} (or R = 1.05) at that level. (Of course, this estimate assumes that the lidar and dustsonde are responsive to the same part of the aerosol size distribution; that is, $N_d = N_a$.) By applying this same model at 11 km, where R is also a minimum and where the dustsonde data are more reliable, $N_d = 0.78$ cm^{-3} corresponds to $f_a = 4.5 \times 10^{-9}$ m^{-1}-sr^{-1} (or R = 1.04). A 5-percent increase in R at the normalization altitude results in a change in f_a at 20 km of about 3×10^{-9} m^{-1}-sr^{-1}, an amount equal to 63 percent of the estimate of f_a itself for a background aerosol layer. Since these aerosol model calculations yield a normalization uncertainty in R of about 5 percent at 30 km, this criterion may be the limiting systematic error in this present inference of absolute concentrations of background stratospheric aerosols by lidar.

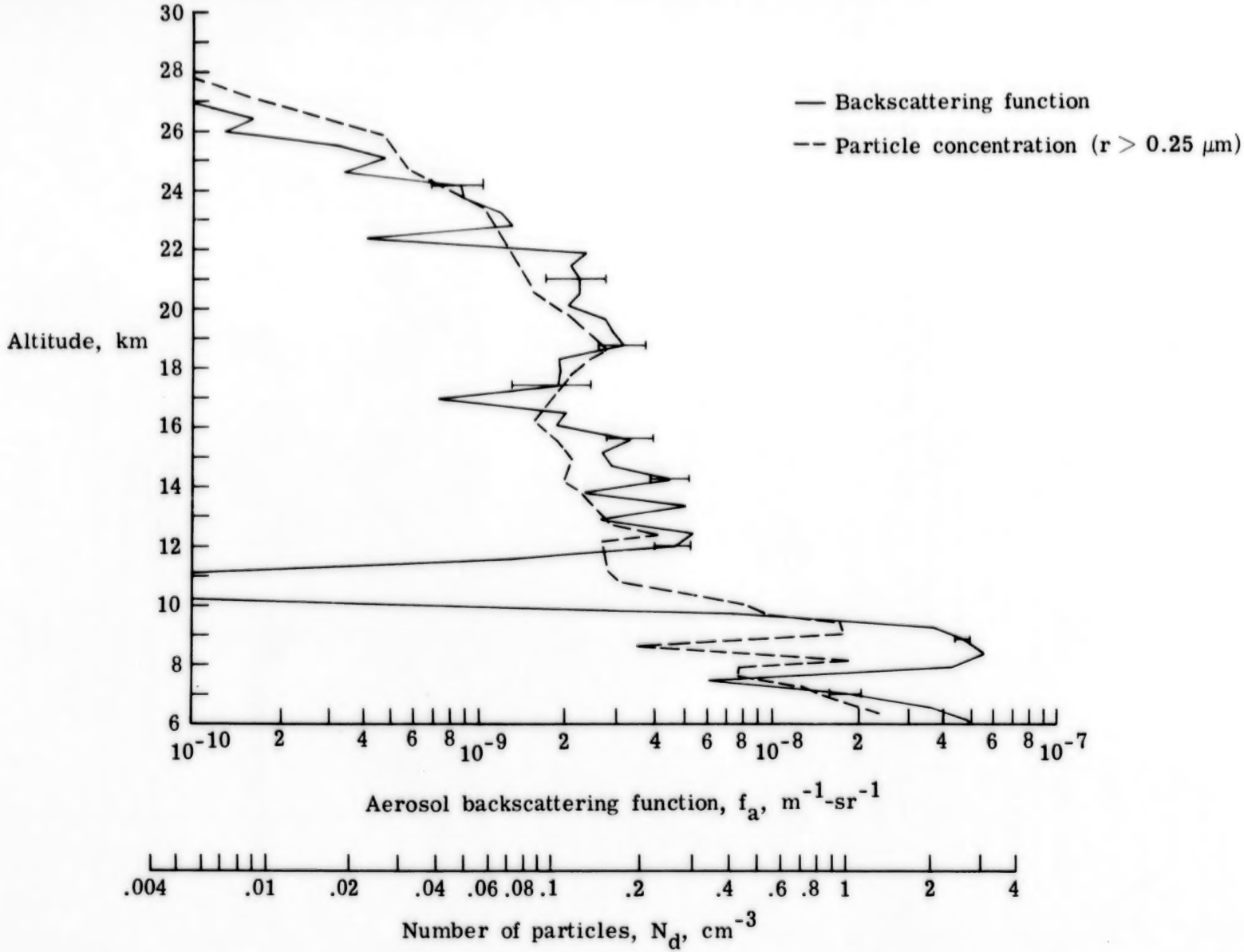

Figure 10.- Comparison of lidar and dustsonde profiles for particles with radii greater than 0.25 μm from TCE.

Effect of Constant Backscatter Cross Section

Data presented in figures 9 and 10 suggest that the normalized lidar measurements more closely approximate the larger particle profile (channel B). The comparison with particles measured by both channels A and B is reasonable up to 23 km; above that altitude, the lidar return seems to underestimate the particle count in channel A.

These results can be analyzed by evaluating the sensitivity of lidar backscatter to various aerosol properties such as the refractive index and the effective cross-sectional area. In early 1974, Russell et al. (ref. 11) compared airborne impactor samples of prevolcanic aerosols to lidar returns at one altitude of 18 km. The refractive index n applied to the aerosol model in that comparison was 1.41 with no imaginary component, consistent with a concentrated sulfuric acid composition. The particles were assumed to be spheres. The assumption of sphericity seems reasonable since Farlow et al. (ref. 15) report collections of only liquid aerosols between 12 and 32 km and for a range

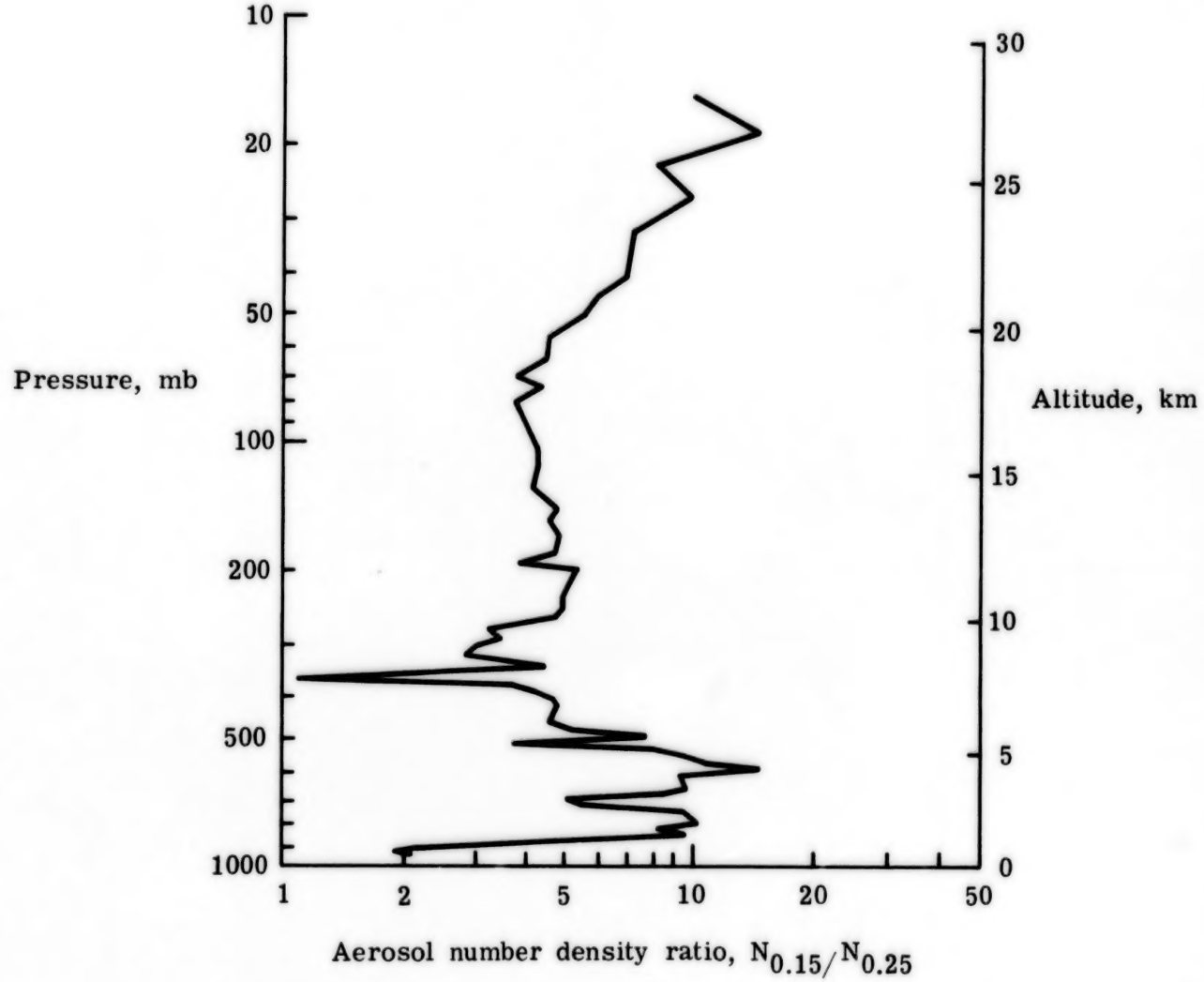

Figure 11.- Profile of aerosol number density ratio from dustsonde launch of May 8, 1974. (See eq. (A4).) 1 mb = 100 Pa.

of latitudes. By applying Mie theory to particles with refractive index 1.41, Russell et al. (ref. 11) calculated aerosol scattering functions which matched their lidar results at 18 km. For determination of aerosol profiles, the possibility of a refractive index change must be considered in σ_a if the aerosol composition varies with height. Lazrus and Gandrud (ref. 16) reported aerosol measurements with height and latitude that showed the predominance of sulfate in the 12 to 28 km region. The bulk of this material is presumed to be concentrated sulfuric acid. Therefore, the TCE scattering ratios above 11 km are assumed to have been affected most by variations due to changes in the particle size distribution rather than changes in composition.

An altitude varying size distribution affects the effective σ_a, which relates backscattered lidar signals f_a and particle number densities N_d. This relation is examined in appendix A, in which the slope of a power-law size distribution function is related to the aerosol number density ratios (channel A divided by channel B) measured by the dustsonde. Aerosol number density ratios for the TCE dustsonde are plotted in figure 11. At all altitudes above 10 km, the aerosol number density ratio is greater than 3.5; from 20 to 28 km, the ratio increases from 4 to 10. An increase of the aerosol number ratio with altitude above the main aerosol layer is normally observed (ref. 17) and can be explained by the theoretical arguments presented by Hamill et al. (ref. 12). The changing number ratio or size distribution causes the lidar backscattering efficiency or the effective f_a ($f_a = \sigma_a N_d$) to decrease with altitude. By multiplying the appropriate efficiency factors γ, derived in appendix A for the data in figure 11, with the curve of N_d in figure 9, a profile of effective f_a is generated. That calculated profile is normalized at 20 km to the profile of measured f_a of figure 9; both profiles are plotted in figure 12. The comparison from 23 to 28 km has been improved by as much as 30 percent. A similar calculation for data in figure 10 (r greater than 0.25 μm) yields an underestimate of f_a above 23 km. Since no data exist on the exact size distribution function for the particles measured during the TCE, the preceding calculations cannot be performed more accurately. Note that this final uncertainty due to $\sigma_a(Z)$ affects both the scattering-ratio profile shape and magnitude, and it can vary with the laser wavelength (σ_a is a function of λ).

The effect of a variable aerosol scattering cross section can be important for volcanic as well as background stratospheric-aerosol layers (ref. 17). However, McCormick et al. (ref. 4) have shown that the bulk of the stratospheric-aerosol backscatter is derived from the region below 23 km, where the aerosol number density ratios are normally less than 3.5. Thus, trends in integrated aerosol column densities for volcanic aerosol layers should not be affected by variations in σ_a with time.

Background Aerosol Attenuation Profile

Turbidity T is a term used to indicate the aerosol loading in the stratosphere. It is defined as the ratio of the aerosol (β_a) and molecular (β_m) total scatter functions, each with dimensions of inverse length; that is,

$$T = \frac{\beta_a}{\beta_m} \tag{3}$$

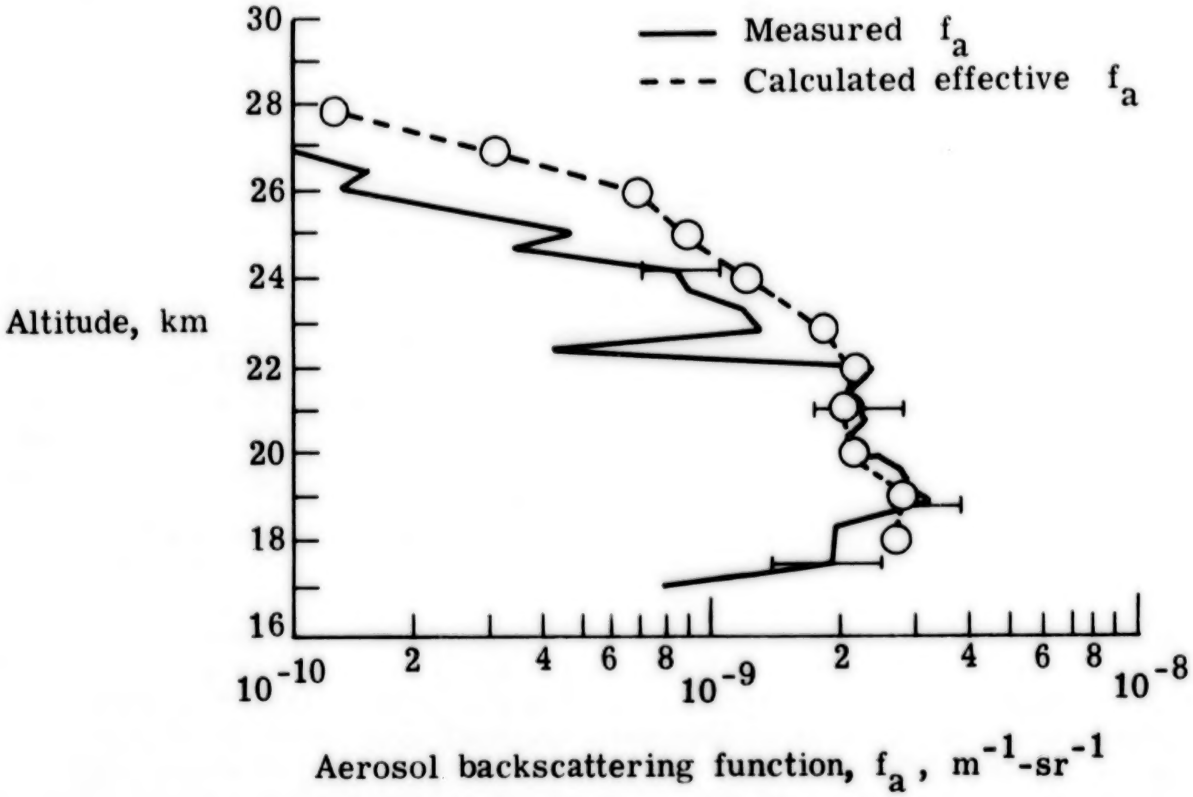

Figure 12.- Comparison between measured and calculated aerosol backscattering-function profiles.

Elterman (refs. 9 and 10) infers turbidity values from his searchlight measurements of attenuation. It is also possible to derive a turbidity estimate and an attenuation profile from the TCE data. The relation, developed in appendix B, between scattering ratio and turbidity for a background aerosol model is written as

$$R = 1.0 + 0.195T = 1.0 + \frac{f_a}{f_m} \tag{4}$$

As shown in appendix B, the coefficient of T in expression (4) depends on the aerosol composition and size distribution. A Deirmendjian Haze H model (ref. 18) of concentrated sulfuric acid was selected as representative of the stratospheric-aerosol layer in May 1974 because it was consistent with the background aerosol estimate of Harris and Rosen (ref. 19) and is equivalent to the power-law size distribution given in appendix A for those particles with radii greater than 0.2 μm.

Reported turbidity values of 1.4 at 20 km prior to the Mt. Agung eruption in the spring of 1963 and of 1.5 in November 1970 (ref. 20) correspond to scattering ratios of 1.27 and 1.29, respectively, for the aerosol model applied in expression (4). The derived scattering ratio for 1970 is somewhat higher than the lidar observations of Fox et al. (ref. 1) and others for 1970 and 1971 (fig. 1), but this could be due partially to the presence of aerosols at normalization altitudes. If we assume that $R = 1.05$ (rather than 1.0) at 28 to 31 km according to our discussion of the normalization uncertainty, then expression (4) applied to the adjusted TCE scattering ratio of 1.12 at 20 km yields a background turbidity of 0.62 for May 1974. Elterman (ref. 21) averaged 113 turbidity profiles obtained over New Mexico from September 1973 to July 1974, showing a value of T of 1.0 at 20 km. However, he reports an aerosol optical thickness between 12 and 25 km for April 1974 that is a factor of 1.3 less than his 10-month average. Therefore, a first-order estimate of his turbidity at 20 km at the time of the TCE is 0.78, or about 25 percent higher than the value inferred from lidar. This discrepancy is well within the absolute error estimates for both f_a and the term $0.195T$ in expression (4).

Scattering-ratio profiles can also be converted to yield aerosol attenuation profiles using the same aerosol model. Profiles of β_a are obtained by combining data from expression (4) with a tabulation of the β_m profiles. If 5 percent of the TCE lidar return signal at 28 to 31 km is assumed due to aerosol ($R = 1.05$), as was estimated in an earlier section, then the curve f_a in figure 9 is adjusted to give the aerosol attenuation profile in figure 13. This profile is offered as an estimate of the aerosol extinction for background stratospheric aerosols.

CONCLUSIONS

Just after the 1972 Wyoming comparative experiment (WCE), a multiplexer was added to the Langley 48-inch lidar system which enabled the recording of a single stratospheric return (10 to 30 km) using three photomultiplier tubes to cover the signal dynamic range. Refinements in the calibration and data-analysis procedures were completed in order to minimize the occurrence of systematic errors. The lidar system generated total stratospheric backscatter signals which when averaged yielded less than 2-percent random counting errors for altitudes up to 30 km and over time periods of less than 1/2 hr. A lidar-dustsonde comparative experiment (TCE) was conducted in May 1974 at San Angelo, Texas, incorporating these updated system calibration and data-analysis procedures. Uncertainties in scattering ratio R induced by the uncertainties in the molecular density profile and the attenuation model were of the order of 0 to 3 percent (average of 1 percent) and less than 1 percent, respectively. Both these uncertainties are assumed to be random. The root-mean-square average of all the random uncertainties is about 2.5 percent. For the TCE, the systematic uncertainty in R due to the clean-air normalization procedure is estimated to be about 5 percent. When these random and systematic uncertainties are applied to the TCE aerosol backscattering function f_a at 20 km, they represent 35 and 63 percent of the value, respectively.

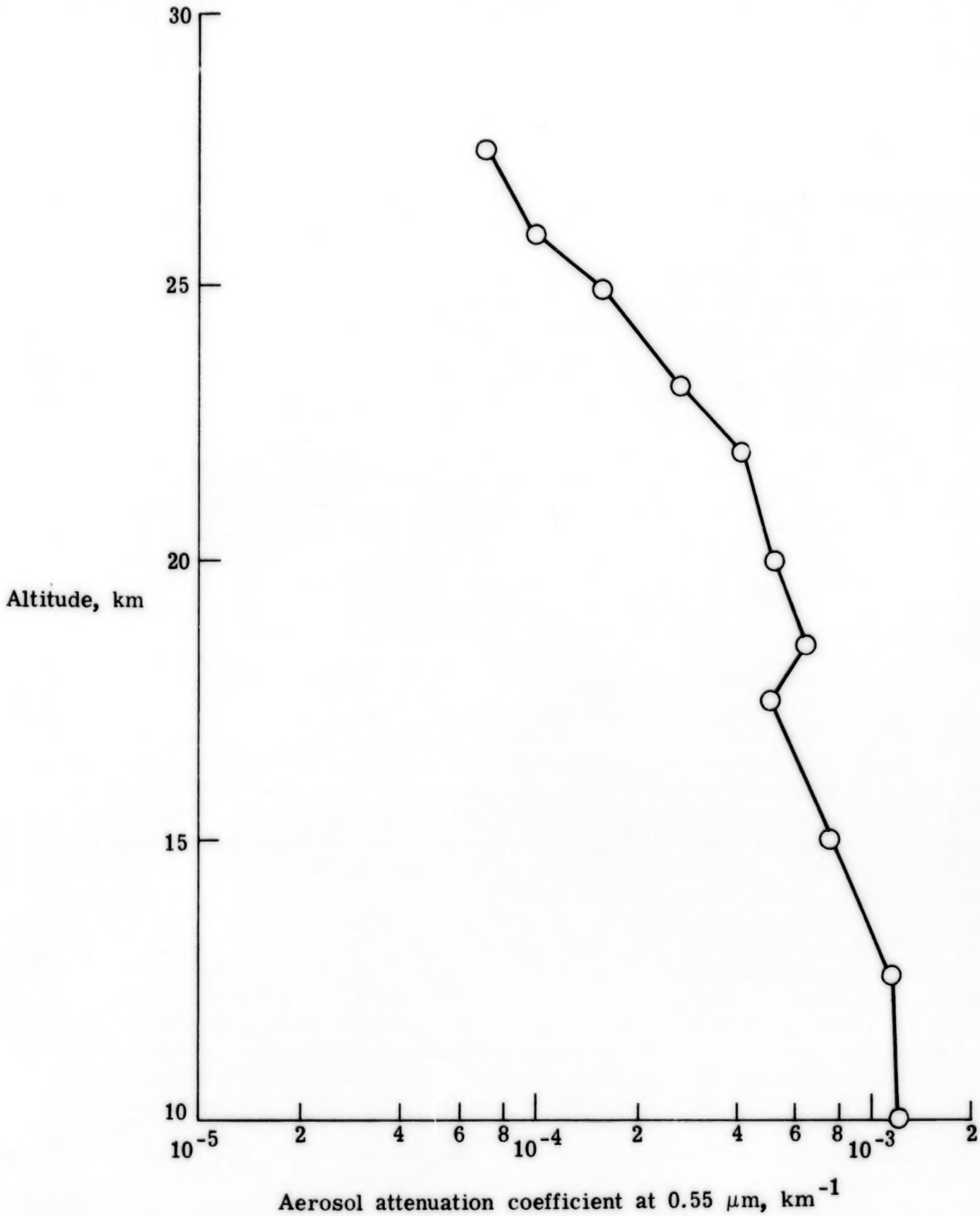

Figure 13.- Profile of aerosol attenuation coefficient derived from TCE.

Comparisons between the dustsonde particle profile N_d and the backscattering profile f_a were within the measurement error bars for the two techniques below 23 km. The two-channel dustsonde data, however, indicate a changing particle size distribution with height. This variation has been applied to the N_d profile with the aid of a realistic aerosol model, and an effective f_a profile was generated. As a result, the comparison between the two f_a profiles is improved by up to 30 percent above 23 km. Since the bulk of the stratospheric-aerosol backscatter is derived from the region below 23 km, this variable size distribution effect is not very important in an analysis of trends in integrated aerosol column density.

The TCE results indicate that individual measurements of scattering ratios above 1.025 can be significant provided that the random uncertainties due to noncoincident molecular-density profiles are avoided. Absolute values of the aerosol backscatter function f_a are further affected by uncertainties in the profile normalization process, and this error must be considered when relative changes (seasonally or yearly variations) in aerosol backscatter are evaluated. Attempts to extend the altitudes from which lidar data are retrieved to greater than 30 km in order to decrease the normalization error are not advised unless methods for obtaining accurate molecular-density profiles from those same levels are also available.

Langley Research Center
National Aeronautics and Space Administration
Hampton, VA 23665
January 11, 1979

APPENDIX A

AEROSOL CROSS-SECTION CALCULATIONS

In order to test the sensitivity of lidar returns to the size distribution, assume a power-law size distribution

$$\frac{dN}{dr} = Cr^{-(\nu+1)} \tag{A1}$$

where N is the number of particles per cm^3, r is particle radius in micrometers, and C is a coefficient proportional to the total number of particles in the size distribution. (A power law is reasonable for 0.1 to 1.0 μm radius particles.) The slope of the distribution is given by the exponent ν. Values (in m^2-sr^{-1}) of the backscattering cross section σ_a are given by the expression

$$\sigma_a = \frac{d\eta}{d\Omega} = \frac{f_a}{N_a} \tag{A2}$$

where Ω is a solid angle and η is the geometric cross section. Values for σ_a are derived from Mie theory as a function of ν and of size parameter α where

$$\alpha = \frac{2\pi r}{\lambda} \tag{A3}$$

Values for σ_a have been tabulated by McCormick et al. (ref. 22) for laser wavelengths. Numerical integrations to obtain $d\eta/d\Omega$ over the size-distribution equation (A1) are performed for a wavelength of 0.694 μm, a refractive index of 1.41, and particle radii limits of r_1 = 0.15 and 0.25 μm to r_2 = 3.0 μm. Sample tabulations are given in table AI.

The size distribution slope ν can be related to the ratio of the number of particles in channel A, represented by $N_{0.15}$, to those in channel B, represented by $N_{0.25}$, as follows:

$$\frac{N_{0.15}}{N_{0.25}} = \frac{\int_{0.15\ \mu m}^{\infty} r^{-(\nu+1)}\,dr}{\int_{0.25\ \mu m}^{\infty} r^{-(\nu+1)}\,dr} \tag{A4}$$

The left-hand side of expression (A4) is determined from measurements of N_d by the University of Wyoming dustsonde, and selected results appear in table AII. Expression (A4) is considered valid, due to the dustsonde measurement technique,

APPENDIX A

TABLE AI.- AVERAGE DIFFERENTIAL CROSS SECTION PER PARTICLE FOR BACKSCATTER

$\nu + 1$	$d\eta/d\Omega$, $m^2\text{-}sr^{-1}$
$r_1 = 0.15$ μm; $r_2 = 3.0$ μm	
3.5	1.52×10^{-14}
4.0	7.77×10^{-15}
4.5	4.50
5.0	2.93
$r_1 = 0.25$ μm; $r_2 = 3.0$ μm	
3.5	5.18×10^{-14}
4.0	3.25
4.5	2.23
5.0	1.66

TABLE AII.- DEPENDENCE OF BACKSCATTER ON SIZE DISTRIBUTION

$\nu + 1$	$N_{0.15}/N_{0.25}$	$(d\eta/d\Omega)_{r>0.15} \Big/ (d\eta/d\Omega)_{r>0.25}$	Relative backscatter efficiency, $\gamma = f_{0.25}/f_{0.15}$
3.45	3.50	0.294	0.97
3.70	4.00	.269	.94
4.00	4.65	.239	.90
4.50	6.00	.201	.83
5.00	7.90	.175	.72
5.50	10.00	.160	.63
6.20	14.20	.143	.49

for particle ratios greater than 3.0 (ref. 13). A lidar aerosol return is determined by the product of the relative backscatter function per particle $d\eta/d\Omega$ and the number of particles N_a. From table AI, one can then form the ratio of that product for each of the two size ranges measured with the dustsonde. As an example, $\nu = 3.0$ corresponds to $N_{0.15}/N_{0.25} = 4.65$ and

$$\left(\frac{d\eta}{d\Omega}\right)_{0.15} \Bigg/ \left(\frac{d\eta}{d\Omega}\right)_{0.25} = 0.24 \tag{A5}$$

The product of the two ratios, equations (A4) and (A5), yields the magnitude of the lidar signal return to be expected from particles in channel A relative to that expected from channel B. The inverse of that product is the relative efficiency for backscatter, $\gamma = f_{0.25}/f_{0.15}$, for the size distributions ratios. When γ is less than 0.5, the ruby lidar receives more signal from the population of particles between 0.15 and 0.25 μm than from the population larger than 0.25 μm.

The power-law size distribution function does not apply so well to particles less than 0.15 μm in radius. Some particle measurement techniques even indicate decreasing or constant particle numbers below about 0.05 μm in radius. Calculations for more realistic distributions of the particles smaller than 0.15 μm indicate that only a very small error is incurred in the above analysis by neglecting them altogether.

APPENDIX B

TURBIDITY CALCULATIONS

A measure of atmospheric particulate loading is the turbidity T, defined as the ratio of the aerosol and molecular total scatter functions

$$T = \frac{\beta_a}{\beta_m} \tag{B1}$$

Turbidity measurements are presented for a wavelength of 0.55 μm in reference 20. They are converted to 0.694 μm to correspond with the lidar results of the present study by

$$T_{0.694} = T_{0.55}\left(\frac{0.694}{0.55}\right)^{2.5} = 1.77T_{0.55} \tag{B2}$$

where β_m varies according to λ^{-4} and β_a varies according to $\lambda^{-1.5}$. The aerosol wavelength dependence is taken from figure 7 of Pinnick et al. (ref. 14). A backscatter turbidity T(180) is measured by lidar and is defined as

$$T(180)_{0.694} = \frac{P(180)}{1.5} T_{0.694} \tag{B3}$$

where 1.5 is the Rayleigh scatter phase function. The aerosol backscattering phase function P(180) is given by Elterman et al. (ref. 20) to be 0.232 for a silicate Deirmendjian Haze H aerosol of refractive index 1.54 (ref. 18), while Russell et al. (ref. 11) use P(180) = 0.165 for a sulfuric acid Haze H model (refractive index of 1.41). Since sulfuric acid is the preferred composition, application of this latter value to equations (B2) and (B3) yields

$$T(180)_{0.694} = 0.195T_{0.55} \tag{B4}$$

The expression for the scattering ratio can be written as

$$R = 1.0 + T(180)_{0.694} = 1.0 + 0.195T_{0.55} \tag{B5}$$

In table BI the sensitivity of the relation between Elterman's turbidity and the scattering ratio is presented by considering three different haze models. Since the coefficient of turbidity varies sharply with the chosen stratospheric model, expression (B5) should only be applied to a relatively unperturbed, nonvolcanic aerosol layer.

APPENDIX B

TABLE BI.- RELATION BETWEEN TURBIDITY AND SCATTERING RATIO

Deirmendjian Haze model (ref. 18)	Refractive index	Coefficient of turbidity, T in equation (B5)
H	1.41	0.195
H	1.54	.274
L	1.41	.263

REFERENCES

1. Fox, R. J.; Grams, G. W.; Schuster, B. G.; and Weinman, J. A.: Measurements of Stratospheric Aerosols by Airborne Laser Radar. J. Geophys. Res., vol. 78, no. 33, Nov. 20, 1973, pp. 7789-7801.

2. Remsberg, Ellis E.; and Northam, G. Burton: A Comparison of Dustsonde and Lidar Measurements of Stratospheric Aerosols. Proceedings of the Fourth Conference on the Climatic Impact Assessment Program, Thomas M. Hard and Anthony J. Broderick, eds., DOT-TSC-OST-75-38, U.S. Dep. Transp., Feb. 1975, pp. 509-518.

3. Russell, P. B.; Viezee, W.; Hake, R. D., Jr.; and Collis, R. T. H.: Lidar Observations of the Stratospheric Aerosol: California, October 1972 to March 1974. Q. J. R. Meteorol. Soc., vol. 102, no. 433, July 1976, pp.675-695.

4. McCormick, M. P.; Swissler, T. J.; Chu, W. P.; and Fuller, W. H., Jr.: Post-Volcanic Stratospheric Aerosol Decay as Measured by Lidar. J. Atmos. Sci., vol. 35, no. 7, July 1978, pp. 1296-1303.

5. Northam, G. Burton; Rosen, James M.; Melfi, S. Harvey; Pepin, T. J.; McCormick, M. P.; Hofmann, D. J.; and Fuller, William H., Jr.: Dustsonde and Lidar Measurements of Stratospheric Aerosols: A Comparison. Appl. Opt., vol. 13, no. 10, Oct. 1974, pp. 2416-2421.

6. McCormick, M. P.; and Fuller, W. H., Jr.: Lidar Techniques for Pollution Studies. AIAA J., vol. 11, no. 2, Feb. 1973, pp. 244-246.

7. Pettifer, R. E. W.: Signal Induced Noise in Lidar Experiments. J. Atmos. & Terrest. Phys., vol. 37, no. 4, Apr. 1975, pp. 669-673.

8. Hunt, W. H.; and Poultney, S. K.: Testing the Linearity of Response of Gated Photomultipliers in Wide Dynamic Range Laser Radar Systems. IEEE Trans. Nucl. Sci., vol. NS-22, no. 1, Feb. 1975, pp. 116-120.

9. Elterman, L.: A Model of a Clear Standard Atmosphere for Attenuation in the Visible Region and Infrared Windows. AFCRL-63-675, U.S. Air Force, July 1963.

10. Elterman, L.: UV, Visible, and IR Attenuation for Altitudes to 50 km, 1968. AFCRL-68-0153, U.S. Air Force, Apr. 1968. (Available from DDC as AD 671 933.)

11. Russell, P. B.; Viezee, W.; Hake, R. D., Jr.; and Collis, R. T. H.: Lidar Observations of the Stratospheric Aerosol: Summary of Results and a Calibration-Error Assessment. Proceedings of the Fourth Conference on the Climatic Impact Assessment Program, Thomas M. Hard and Anthony J. Broderick, eds., DOT-TSC-OST-75-38, U.S. Dep. Transp., Feb. 1975, pp. 497-508.

12. Hamill, Patrick; Toon, O. B.; and Kiang, C. S.: Microphysical Processes Affecting Stratospheric Aerosol Particles. J. Atmos. Sci., vol. 34, no. 7, July 1977, pp. 1104-1119.

13. Hofmann, D. J.; Rosen, J. M.; Pepin, T. J.; and Pinnick, R. G.: Stratospheric Aerosol Measurements I: Time Variations at Northern Midlatitudes. J. Atmos. Sci., vol. 32, no. 7, July 1975, pp. 1446-1456.

14. Pinnick, R. G.; Rosen, J. M.; and Hofmann, D. J.: Stratospheric Aerosol Measurements III: Optical Model Calculations. J. Atmos. Sci., vol. 33, no. 2, Feb. 1976, pp. 304-314.

15. Farlow, Neil H.; Hayes, Dennis M.; and Lem, Homer Y.: Stratospheric Aerosols: Undissolved Granules and Physical State. J. Geophys. Res., vol. 82, no. 31, Oct. 20, 1977, pp. 4921-4929.

16. Lazrus, A. L.; and Gandrud, B. W.: Stratospheric Sulfate Aerosol. J. Geophys. Res., vol. 79, no. 24, Aug. 20, 1974, pp. 3424-3431.

17. Hofmann, D. J.; and Rosen, J. M.: Balloon Observations of the Time Development of the Stratospheric Aerosol Event of 1974-1975. J. Geophys. Res., vol. 82, no. 9, Mar. 20, 1977, pp. 1435-1440.

18. Deirmendjian, D.: Electromagnetic Scattering on Spherical Polydispersions. American Elsevier Publishing Co., Inc., 1969.

19. Harris, Franklin S., Jr.; and Rosen, James M.: Measured and Analytic Distributions of Stratospheric Aerosols: A Review and Commentary. Atmospheric Aerosols: Their Optical Properties and Effects, NASA CP-2004, 1976, pp. MA2-1-MA2-4.

20. Elterman, Louis; Toolin, Robert B.; and Essex, John D.: Stratospheric Aerosol Measurements With Implications for Global Climate. Appl. Opt., vol. 12, no. 2, Feb. 1973, pp. 330-337.

21. Elterman, Louis: Aerosol Measurements Since 1973 for Normal and Volcanic Stratospheres. Appl. Opt., vol. 15, no. 5, May 1976, pp. 1113-1114.

22. McCormick, M. P.; Lawrence, J. D., Jr.; and Crownfield, F. R., Jr.: Mie Total and Differential Backscattering Cross Sections at Laser Wavelengths for Junge Aerosol Models. Appl. Opt., vol. 7, no. 12, Dec. 1968, pp. 2424-2425.

1. Report No.	2. Government Accession No.	3. Recipient's Catalog No.
NASA TP-1381		

4. Title and Subtitle	5. Report Date
LIDAR BACKSCATTERING MEASUREMENTS OF BACKGROUND STRATOSPHERIC AEROSOLS	February 1979
	6. Performing Organization Code

7. Author(s)	8. Performing Organization Report No.
Ellis E. Remsberg, G. Burton Northam, and Carolyn F. Butler	L-12292
	10. Work Unit No. 198-30-02-05
9. Performing Organization Name and Address	11. Contract or Grant No.
NASA Langley Research Center Hampton, VA 23665	
	13. Type of Report and Period Covered
12. Sponsoring Agency Name and Address	Technical Paper
National Aeronautics and Space Administration Washington, DC 20546	14. Sponsoring Agency Code

15. Supplementary Notes

Ellis E. Remsberg and G. Burton Northam: Langley Research Center.
Carolyn F. Butler: Old Dominion University Research Foundation, Norfolk, Virginia.

16. Abstract

A comparative lidar-dustsonde experiment was conducted in San Angelo, Texas, in May 1974 in order to estimate the uncertainties in stratospheric-aerosol backscatter for the NASA Langley 48-inch lidar system. The lidar calibration and data-analysis procedures are discussed. Results from the Texas experiment indicate random and systematic uncertainties of 35 and 63 percent, respectively, in backscatter from a background stratospheric-aerosol layer at 20 km.

17. Key Words (Suggested by Author(s))	18. Distribution Statement
Stratospheric aerosols Lidar measurements	Unclassified - Unlimited Subject Category 46

19. Security Classif. (of this report)	20. Security Classif. (of this page)	21. No. of Pages	22. Price*
Unclassified	Unclassified	32	$4.50

* For sale by the National Technical Information Service, Springfield, Virginia 22161

NASA-Langley, 1979

END

Sept. 14, 1979